ORIGINAL ARTICLES

A semiautomatic tracking algorithm for mitral annular plane excursion: A mode for cardiac function evaluation

Uri Goldsztejn*[1], Hadas Avraham[1], Grigoriy Zurakhov[1], Hanan Khamis[1], Zvi Friedman[2]

[1] *Laboratory for Ultrasound Signal and Image Processing and Modeling, Faculty of Biomedical Engineering, Technion Israel Institute of Technology, Haifa, Israel*
[2] *GE Ultrasound, Tirat Hacarmel, Israel*

Received: December 22, 2016 **Accepted:** February 14, 2017 **Online Published:** March 26, 2017
DOI: 10.5430/jbei.v3n2p11 **URL:** https://doi.org/10.5430/jbei.v3n2p11

ABSTRACT

Reduced long-axis deformation as derived from the temporal excursion of the mitral annular plane correlates well with left ventricle systolic and diastolic dysfunction. Since this parameter is barely compensated at the onset of ventricular dysfunction, it is proposed as an early marker of a dysfunction. The lack of a rapid, yet accurate tool for the evaluation of mitral annular plane excursion (MAPE) prevents this measurement from being used routinely in the clinic. Here, a semiautomatic tracking algorithm of the mitral annulus was developed. Describing the MAPE in clear geometrical terms together with state-of-the-art speckle tracking and speckle reduction algorithms, facilitated the development of such an algorithm. The performance of the algorithm was evaluated using a cohort of 48 apical views of subjects chosen randomly from a set of routine examinations done at Rambam Hospital. The curves obtained using the proposed algorithm were compared using a cross-correlation test with the standard global strain. The average cross-correlation coefficient obtained was 0.92, with standard deviation of 0.07.

Key Words: Mitral Annular Plane Excursion (MAPE), Block matching, Strain curves, Mitral valve, Recovery assessment

1. INTRODUCTION

Ultrasound imaging is a widely accepted technique for the assessment of myocardial function. The left ventricular ejection fraction (LVEF) and stroke volume (SV) are commonly used as diagnostic parameters of cardiac dysfunction. However, these parameters are constantly regulated through various mechanisms; therefore, their values reflect the myocardial condition together with the current physiological demand.[1–3] This leads to significant variability between subjects and between measurements of different exams of the same subject.[4]

The mitral annular plane excursion (MAPE) with respect to the cardiac apex has been proposed as an alternative parameter for assessing myocardial function.[5] It reflects the longitudinal contraction and relaxation of the myofibers.[6,7] The following characteristic of the longitudinal contraction has motivated this work. Impairments in longitudinal contraction are not directly compensated but corrected by means of changes in radial and circumferential function.[8] The fact that MAPE is not regulated at the onset of cardiac disease as opposed to the LVEF or the SV, allows using it as an early marker of various pathologies.[4,9] MAPE has been

*Correspondence: Uri Goldsztejn; Email: urisaad@gmail.com; Address: Lab for Ultrasound Signals and Image Processing and Modelling, Department of Biomedical Engineering, Technion, Haifa, Israel.

proposed[4] as an early marker of heart failure, dilated cardiomyopathy, hypertrophic cardiomyopathy, and valvular, diabetic, hypertensive and ischemic heart diseases. MAPE has also been proposed for close follow-up after myocardial infarction.[10] This would allow objective estimation of heart remodeling during the crucial period following myocardial infarction.

Although the relevance of MAPE has been proved and accepted, it is still not commonly used in the clinic. The main reason may be the lack of a simple, yet accurate built in tool for assessing MAPE. Since a manual detection of the mitral annular plane in each frame of an echocardiogram is not feasible in the clinic, several semiautomatic tracking algorithms have been proposed. Two main approaches for tracking the motion of the mitral annulus throughout the cardiac cycle have been explored. The first approach is based on forward tissue tracking.[11] This method is useful for motion tracking in applications with relatively low levels of noise (e.g. for following objects from the air) but tends to drift away from the correct trace in echocardiograms. The second approach relies on more computationally demanding techniques. Good results have been obtained using a dynamic programming based algorithm.[12] However, this algorithm has been implemented only for tracking the mitral valve in apical four chamber (A4C) echocardiograms and was tested only in patients with acute myocardial infarction and not with randomly selected subjects. Additionally, reported computation times are of about two minutes for single cycle echocardiograms, recorded with a frame rate of 25 fps.

Computation time is an important factor for implementing new tools in the clinic. A multidimensional dynamic programming approach would require several minutes for a single heart cycle echocardiogram with the frame rate used in this work (about 70 fps). This frame rate is usually used in routine echocardiograms, but higher frame rates should be used (> 100 fps)[13] for optimal results. Besides, as ultrasound imaging devices are improved, the frame rate, and therefore the number of frames per single heart beat increase, making the algorithm impractical for routine clinical use.

The algorithm developed in this paper is both not computationally demanding, as it can be executed on any modern ultrasound workstation along other algorithms, and can produce accurate results. A block matching approach was used for tracking the mitral valve in a gradient domain taking advantage of the low computation time of this approach. The movement is conditioned based on anatomical information obtained from the echocardiogram and different points are concomitantly tracked for optimal results.

2. METHODS

The proposed algorithm consists of the following steps: the input frames of each video were first pre-processed for noise reduction, and then underwent gradient extraction. Each pixel, of every frame, was assigned a phasor composed of the magnitude and direction of its gradient. The operator was requested to select a set of initial points in the raw data, whereas the noise reduction and gradient extraction run in the background. The left subendocardial basal and mitral valve points are selected both in the first and in the last frames, as depicted in Figure 1. The selection in the last frame is used for a backward tracking, as will be explained in section 2.4 below. The position of the left subendocardial basal point is then iteratively searched between frames using a block-matching algorithm.[11] The MAPE trace is then calculated as the distance from the left subendocardial basal point to the subepicardial apex. The subepicardial apex is assumed to remain fixed along the clip.[14]

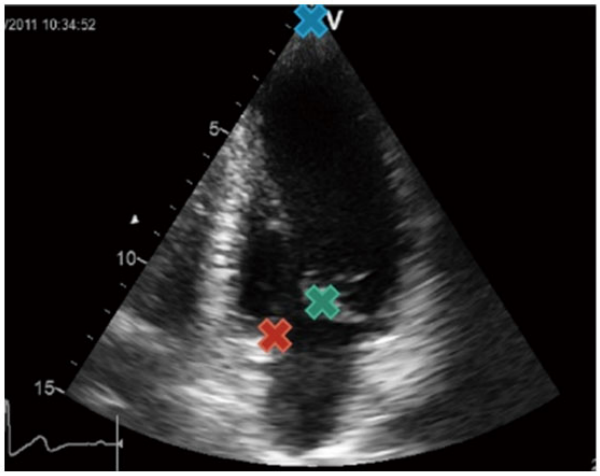

Figure 1. The operator is requested to mark the subepicardial apex (blue), a point on the mitral valve (green) and the left subendocardial basal point (red) only in the first frame

A point on the mitral valve is selected to identify the frames in which it opens and closes. From this information, the cardiac cycle can be divided into different phases (as explained in section 2.2). This feature allows to define different tracking parameters for each phase. This advantage is what makes the algorithm work in both apical two and four chamber echocardiographic views.

Since the point on the mitral valve is used only to determine whether the valve is opened or closed, its precise location is irrelevant as long as it lies around the middle of the valve in the initial frame. Slight differences in its initial location do not lead to different results.

2.1 Preprocessing

In order to account for the variations of the input image quality and sampling parameters, a robust data preprocessing is employed. B-Mode ultrasound images are characterized by speckles originated from the diffusive nature of the scatterers that are much smaller than the pulse central wavelength. Since the developed algorithm operates in the gradient domain, speckles which behave as a high frequency noise, disrupt its performance. Thus, it's crucial to attenuate speckle noise while preserving enough information for the tracking algorithm.

Since this work relies heavily on image gradients it is desired to reduce the speckles which behave as high frequency texture noise. Over the years, several filters have been proposed for despeckling of ultrasound B-Mode images, including the state-of-the-art Non-Local means filter.[12, 13] In this work the filters described and compared in the work by Loizou et al.[15] and the Non-Local means filter implemented by Coupe et al.[16] were considered. This last filter provides a greater smoothing effect and better preserves the edges but requires a computation time around eight times larger than that required by the filters proposed by Loizou et al.

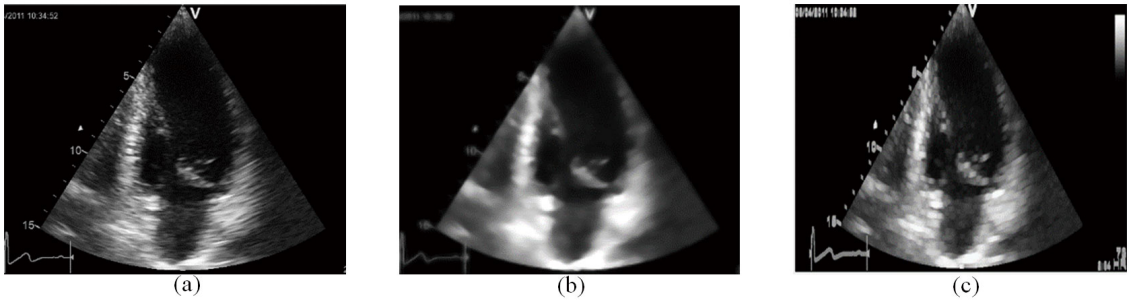

(a) (b) (c)

Figure 2. (a) A sample frame as obtained from a routine apical two chamber view echocardiogram. (b) The same frame after despeckling using a Non-Local means filter. (c) The same frame after despeckling using the Geometric despeckle filter (DsFgf4d)

To choose a filter for our work, the tracking algorithm was run on videos despeckled with the different filters. With the exception of the Linear despeckle filter (DSFIsmv), all led to similar results. The Linear despeckle filter barely removed the speckles and led to erratic traces. For this work, the filter chosen was the Geometric despeckle filter (DsFgf4d) since its computation time is fifteen times faster than the Non-local means filter. Although the Geometric despeckle filter is not well ranked, it solves the speckle issue for our algorithm. More refined filters improve the image appearance but are beyond the requirements of the proposed tracking algorithm.

Table 1. Computation time of different despeckling filters.[14]

Filter	Computation time [s]
DSFIsmv	0.18
DsFgf4d	0.55
DsFhomog	1.36
DsWavletC	1.69
DsFca	1.21
DsFsrad	1.71
DsFmmedioan	1.80
DsFlsminsc	7.24
Non-Local means filter	8.57

In Table 1, the right column lists the computation time required to process a single frame.

The computation time for the chosen despeckling filter was on average 16 seconds per clip with a standard deviation of 3.5 seconds (this variability can be attributed to the slight differences in the clip lengths).

The preprocessing step contributes significantly to the robustness of the algorithm by differentiating the real edges from the speckle noise, an obstacle that may lead to the drifting of the tracking from the correct path.

2.2 Gradient extraction

In order to extract only the information required for the tracking itself, all despeckled frames of the video were transformed into a complex matrix. In this matrix, each pixel is represented as a phasor having an amplitude, equal to the magnitude of the gradient in the source frame ($|\bigtriangledown \cdot Img(x,y)|$) and by a phase $(\measuredangle(\nabla \cdot Img(x,y)))$, that represents its direction.

The phasor is thus defined as:

$$Img^{G}(x,y) = |\nabla \cdot Img(x,y)| \cdot e^{j\cdot\measuredangle(\nabla\cdot Img(x,y))} \quad (1)$$

The image gradient domain is defined as the image in which

the value of every pixel is switched for its corresponding phasor. This operation clearly separates the edges from the rest of the tissue (see Figure 3).

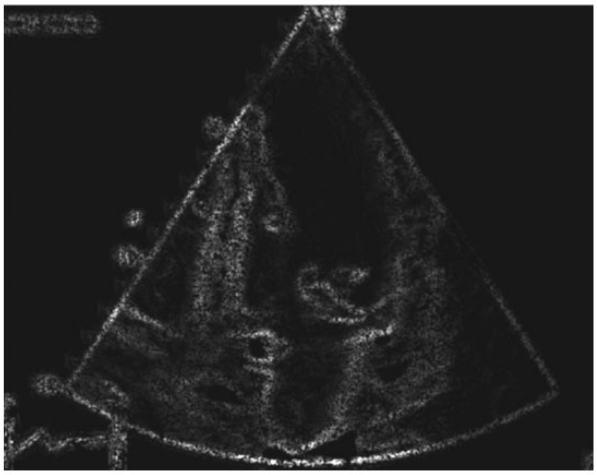

Figure 3. The first frame of a sample echocardiogram after complex gradient extraction. Only the amplitude of the image gradient domain is shown.

For optimal tracking, the video representing a single heart cycle is divided into four phases according to the expected MAPE motion direction. The pertinent phases are:

(1) Systole–the mitral annulus moves towards the apex.
(2) Diastole–the mitral annulus moves away from the apex.
(3) Plateau–there is no longitudinal relative motion between the apex and the mitral annulus.
(4) Atrium contraction–the mitral annulus moves away from the apex.

These phases are identified according to the mitral valve opening and closing. The transient state of the mitral valve is found from the sum of the intensities around the initially selected point (a closed valve will be bright leading to a high intensity). The relation between the state of the valve and the phase of the heart cycle is presented (see Figure 4). There is a small delay between the changes in phase between the two graphs which is a result of the delay in the response of the mitral valve to changes in the pressure gradient between the left atrium and ventricle. This delay varies between subjects and is related to the flexibility of the valve leaflets. The delays observed in our data set were between 5 and 15 percent of the heart cycle duration. The tracking is done assuming a range of possible delays and, the best result is chosen in the validation phase.

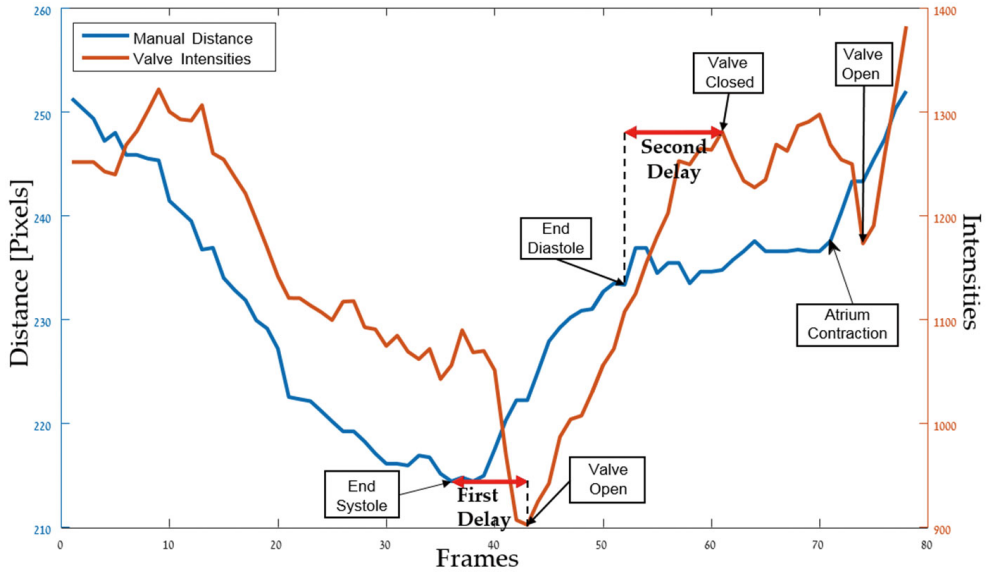

Figure 4. The intensity measured around the initial position of the mitral valve (in red) is minimal when the valve is open and maximal when it is closed. A local minimum in the intensity is observed during the atrial kick, when the mitral valve opens slightly. The MAPE (in blue) was manually marked. The MAPE phases correlate well with the phases of the intensities up to the unknown delays.

2.3 Block matching

The tracking algorithm developed is based on block matching, a technique for motion tracking common in computer vision.[16] This technique was implemented in the complex gradient domain, while the operator interacts only with the original video.

A region of interest (ROI_i) is defined as a 3×3 patch around the initial basal point position, manually marked by the operator. At the same time, a region of search (ROS_{i+1}) is defined in the consecutive frame around the ROI_i. In the newly defined ROS_{i+1}, the 3×3 patch that most closely resembles the previous ROI_i is searched. It is then defined to be the new ROI_{i+1}. The procedure is performed consecutively for all frames.

The ROS_{i+1} is defined around the previous position of the basal point (ROI_i) and its dimensions depend on the current physiological phase (see Table 2 and Figure 5).

Table 2. ROI's dimensions

Physiological phase	L [pixels]	M [pixels]	N [pixels]
Systole	2	5	3
Diastole	2	2	6
Plateau	2	3	3
Atrium contraction	2	2	4

Three modalities are proposed for finding the ROS_{i+1} is in the ROS_{i+1} is. The first is based on correlations, where the ROS_{i+1} is is defined as the area in the ROS_{i+1} is that maximizes the Pearson correlation coefficient (r) with respect to ROI_i.

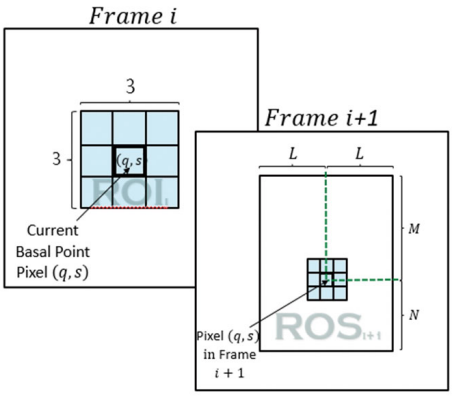

Figure 5. An illustration for Table 1. L, M and N define the dimensions of the ROS_{i+1} around the ROI_i. The ROI_i is horizontally centered in the ROS_{i+1} and L indicates the distance (in pixels) from the center of the ROI_i to the vertical edges of the ROS_{i+1}. M and N indicate the distance (in pixels) from the center of the ROI_i to the upper and lower edges of the ROS_{i+1}, respectively.

The Pearson correlation coefficient is defined as:

$$r = \frac{\sum_{h=-1}^{1}\sum_{k=-1}^{1}(Img_{i+1}(q'+h,s'+k) - \overline{Img_{i+1}})\,(Img_i(q+h,s+k) - \overline{Img_i})}{\sqrt{\sum_{h=-1}^{1}\sum_{k=-1}^{1}(Img_{i+1}(q'+h,s'+k) - \overline{Img_{i+1}})^2 \sum_{h=-1}^{1}\sum_{k=-1}^{1}(Img_i(q+h,s+k) - \overline{Img_i})^2}} \tag{2}$$

Where (q, s) and (q', s') are the positions of the basal points in frames i and $i+1$, respectively. The expression was evaluated for every (q', s') in the ROS_{i+1}. $\overline{Img_{i+1}}$ and $\overline{Img_i}$ are the average value of the pixels in the candidate ROI and the current ROI, respectively.

Then the following optimization problem is defined for each frame.

$$(q', s')_{optimal} = \max_{(q', s')} r \tag{3}$$

Where $(q', s')_{optimal}$ is the position in the in the ROS_{i+1} that maximizes the correlation between the 3×3 patch around (q', s') and the ROI_i. By solving this optimization problem for each frame, a series of positions $(q'_i, s'_i)_{optimal}$ is obtained. This series is the MAPE.

The second modality to obtain the MAPE is the Sum of Absolute Differences (SAD). According to this criterion, the new ROI_{i+1} is centered around the position (q', s') that solves the following optimization problem:

$$(q', s')_{opt} = \min_{(q', s')} \theta(q', s') \cdot \sum_{h=-1}^{1}\sum_{k=-1}^{1} |Img_{i+1}(q'+h, s'+k) - Img_i(q+h, s+k)| \tag{4}$$

This optimization problem is then solved for each frame, as in the case of the correlations criterion, and the MAPE is obtained as a series of positions $(q'_i, s'_i)_{optimal}$.

$\theta(q', s')$ is a weighting parameter, defined to give preference to expected motion directions according to the current physiological phase (see Table 3).

Another known modality for template matching is the Sum of Squared Differences (SSD), which is defined similarly to the SAD:

$$(q',s')_{opt} = \min_{(q',s')} \theta(q',s') \cdot \sum_{h=-1}^{1} \sum_{k=-1}^{1} \left(Img_{i+1}(q'+h,s'+k) - Img_i(q+h,s+k)\right)^2 \tag{5}$$

Table 3. Definition of the cost function $\theta(q', s')$

$\theta(q', s')$	Physiological phase	Movement with respect to apex	Displacement [pixels]
0.9	Systole	Towards	Less than 3
0.9	Diastole	Away	More than 2
0.9	Plateau	None	Less than 4
0.9	Atrium contraction	Away	Indifferent
1	Else	Else	Else

Description: When the three relevant conditions hold, $\theta(q', s') = 0.9$, otherwise $\theta(q', s') = 1$. This function imposes a preference for certain directions by altering expression (4). For example, if the current physiological phase is systole (column two), the movement of the basal point towards the apex (column three) and the displacement (column four) between consecutive frames is less than three pixels, the cost function $\theta(q', s')$ evaluates to 0.9. However, if the displacement is 4 pixels, the cost function would evaluate to 1, thus favoring the expected movements.

Unlike the work by Nevo et al.[12] which used the correlations modality, the SAD was chosen here. The SAD modality was chosen since low correlation coefficients were observed at phase changes (e.g. from the end of the systole to the beginning of the diastole). This phenomenon can be explained by the twist of the heart as it compresses. When diastole starts, the twisting movement is in the opposite direction, leading to a considerable discontinuity in the phasors' distribution around the basal point. This effect leads to erroneous choices of the ROI_{i+1}. This phenomenon was less common when using the SAD modality. Moreover, the SAD modality has a lower computation cost.

However, there are disadvantages to the SAD modality, since it is less accurate when the movement is along straight traces. This does not present a major problem since the tracking along straight traces is relatively simple. The summation modality yields very similar results to those of the correlations modality along straight traces.

SAD was chosen over the SSD modality since the tracking takes place on the image gradient domain, where the pixels take complex values (phasors).

2.4 Reverse tracking

Errors accumulate in the successive iterations, which cause some of the traces to deviate from the manual tracking at the last frames.[17] To overcome this problem, a reverse tracking is performed in addition to the forward tracking. The order of the frames is reversed, and the algorithm is run again with the points initially selected in the last frame.

After a forward and reverse trace are obtained, the two traces are combined. In the frames corresponding to systole and atrial contraction, only the forward and reverse traces, respectively, are used.

For the remaining phases, a weighted average is used to build an optimal trace. The trace which began at the last frame is weighted by 0.6, while the forward trace is weighted by 0.4. This combination was found to be optimal for most cases. The cost function used for determining this values was the discontinuity obtained at the connection of the traces. In the phases where only one tracking (forward or reverse) takes place, the accumulated error is assumed to be negligible, and therefore, correct. In accordance with this, the combined trace obtained for the section in between is required to match the forward and reverse traces.

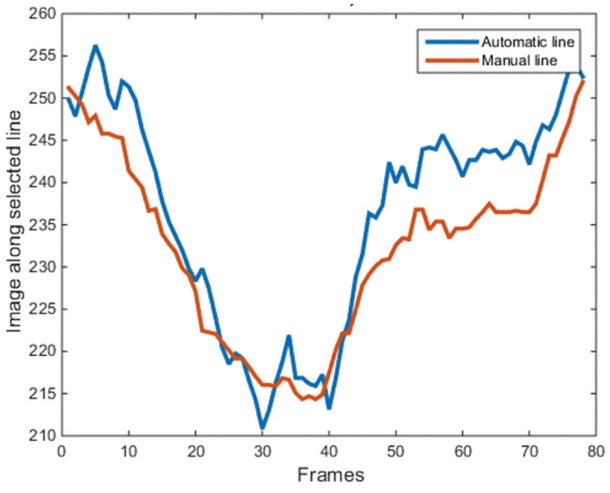

Figure 6. The MAPE obtained automatically is shown in blue while that marked manually is shown in red. Notice that the error increases towards the last frames. The Reverse tracking was implemented to correct these cases. The correlation between the curves shown is 0.96.

In Figure 6, a MAPE trace obtained in a case in which the errors accumulate towards the end is presented.

2.5 Multiple initial positions

A common problem of tracking algorithms is the sensitivity to the selection of the initial position. During the development stage, it was appreciated that occasionally an offset of only a few pixels in the initial position could lead to wrong traces. This happens when the ROI around the selected initial position does not include the edge of the tissue.

To solve this issue, four additional points (above, below, to the right and to the left of the initial position) are tracked. These points were initially defined as a 3 pixel translation from the manually defined initial position which leads to several possible traces, one for each different initial point and possible delay combination. To choose the optimal trace from those obtained, a correlations score was defined. For each trace obtained, the correlations between successive ROIs are added to give the correlations score. The ROIs considered here are in the image domain. Then the trace with the highest correlations score is chosen and presented.

This method ensures that our algorithm gives results in accordance to those obtained using speckle tracking.[18] The speckle tracking technique is based on the idea that the speckles seen in echocardiograms are not only generated by a stochastic process related to the data acquisition but also by tissue discontinuities.[19] Tracking algorithms have been proposed based on the idea that since the discontinuities are embedded within the tissue, they move together with it.[20] One of the main difficulties encountered in those algorithms is to distinguish between noise and a signal of similar characteristics.

To estimate the strength of speckle tracking, correlations between ROIs along manually marked traces and erroneous ones were analyzed in the original video domain (before the preprocessing stage). The correlations modality was used here since repeated patterns were looked for in different frames. In virtually all the cases, the sum of correlations along the manually marked trace was considerably higher than the sum along erroneous traces. Nonetheless, in several steps along the manually marked trace, low and even negative correlations were observed. This makes the speckle tracking a very problematic approach for motion tracking but useful for trace validation, as used here.

3. Results

Cross-correlations between manually marked traces and those produced by the algorithm were used to assess the accuracy of the results obtained. During the development phase, the algorithm's parameters were optimized so that the traces obtained matched the manually marked traces used as a train set (n = 10) (see Figure 7). To evaluate the performance of the algorithm a new data set of two and four chambers (n = 48) was used, one clip per subject was analyzed. Cross-correlations were 0.88 $\pm$ 0.07, range [0.73, 0.97] [2Ch. views (n = 23)] and 0.87 $\pm$ 0.06, range [0.72, 0.96] [4Ch. views (n = 25)].

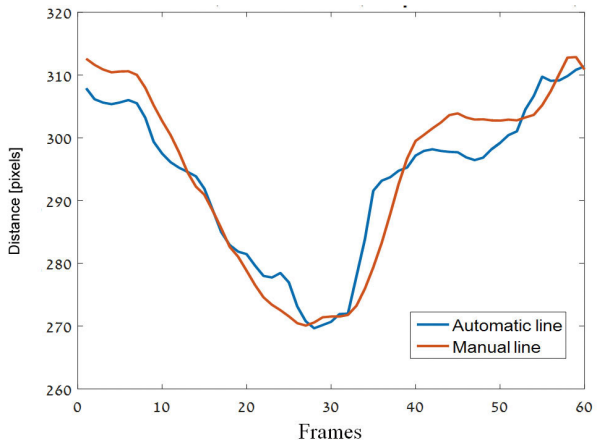

Figure 7. Automatically obtained MAPE trace (blue) and the corresponding manual trace (red). The cross-correlation between the curves is 0.96.

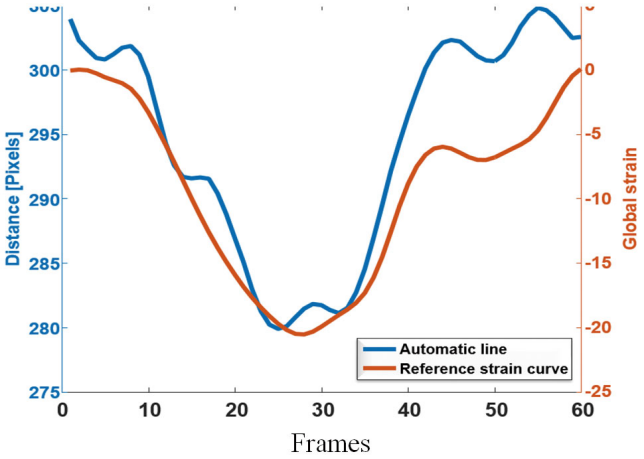

Figure 8. Comparison of the MAPE trace obtained with the proposed algorithm with the 2D global strain curve obtained for the same clip. Although 2D global strain curves measure the average relative contraction of the tissue instead of the MAPE, both curves are related by an approximately constant factor. The cross correlation between the curves shown is 0.95.

MAPE traces have been proposed as an initial measurement to derive 2D global strain curves.[21] While 2D global strain

curves have been shown to accurately reflect the heart condition,[22,23] its measurement requires good quality clips and complex algorithms. The complexity of these algorithms stems from the derivation of the 2D strain curves from tracking the whole left ventricle concomitantly.[24] MAPE traces on the other hand, do not require high quality clips and can be obtained efficiently with the algorithm proposed here.

The traces obtained were compared using cross-correlations with 2D global strain curves obtained with commercial software developed by GE Healthcare. Cross-correlations were 0.94 ± 0.04, range [0.75, 0.98] [2Ch. views (n = 23)] and 0.90 ± 0.08, range [0.61, 0.97] [4Ch. views (n = 25)]. These high correlations support the idea that MAPE traces can be used to derive 2D global strain curves.

4. Discussion

The algorithm presented in this paper has been shown to track the MAPE accurately and time efficiently. However, it does contain several fixed parameters that were not optimized due to the limited size of our data set. It is left for a future work to optimize those parameters according to the cost functions described with a significantly larger data set, for example defining the despeckling parameters that are optimal for tracking rather than for a clinical analysis.

Although the algorithm was coded in MATLAB, it was optimized for improved computation times. Parallelization was implemented, taking advantage of the different cores available in modern processors. The average running time of the despeckling and tracking is 8.6 seconds per video with a standard deviation of 2.4 seconds, running on an Intel Core i7 at 2.40 GHz with 16 GB RAM. The despeckling algorithm was also implemented in CPP but no significant computation time improvements were obtained. A GPU implementation can be considered for further execution time improvement.

The developed algorithm provides more accurate traces than those obtained with minimal and forward tracking,[25] but with slightly increased computation times. Multidimensional dynamic programing[12] is a more robust technique and much more time consuming method.[22] The computation times reported for multidimensional dynamic programing[12] makes the real time application of this approach more difficult. The algorithm developed here provides results comparable to those obtained with multidimensional dynamic programing with much lower computation times.

The current study is limited by the size of the available data set. A larger data set may likely improve the algorithm's parameters tuning and inaccuracy analysis. Additionally, in order to include the algorithm in the clinical data analysis pipeline, it needs to be validated against a larger number of patients (which introduces more variations in the input data). While this study used a small data set, its results indicate the high potential of the developed algorithm and encourage further research on a larger data set.

5. Conclusions

The goal of this work was to develop a reliable tool for automatic MAPE computation. The obtained results support the implementation of the developed algorithm in commercial ultrasound equipment. The traces obtained correlate well with manually marked traces. Additionally, the results obtained were similar for both two and four chambers echocardiograms of randomly selected patient cohorts.

Moreover, since algorithms used to obtain 2D global strain curves are usually computationally complex the presented algorithm is suggested as an alternative.

The echocardiograms used in this work were anonymous and not classified according to pathologies. Dilated atria and left ventricles were observed, suggesting functional abnormalities in some of the patients. Nonetheless, no expert inspected the echocardiograms. It is left for future work to verify the presented algorithm in patients with different cardiac functionalities and evaluate the results according to different pathologies.

This work constitutes a bridge between previous work on MAPE and the clinic. It will allow modern equipment to implement MAPE for routine clinical use. Additionally, it will facilitate further research into the use of MAPE as a diagnostic tool. It would allow research into other proposed longitudinal function assessment uses, such as diagnosis of pulmonary emboli. Pulmonary emboli's assessment from right ventricle longitudinal contraction reduction has been suggested.[26,27] The developed algorithm may be adapted for the right ventricle and used as a tool for diagnosis of pulmonary emboli.

References

[1] Barcarse E, Kazanegra R, Chen A, et al. Combination of B-Type Natriuretic Peptide Levels and Non-Invasive Hemodynamic Parameters in Diagnosing Congestive Heart Failure in the Emergency Department. Congest Heart Fail. 2004 Jul 1; 10(4): 171-6.

[2] Borlaug BA, Melenovsky V, Russell SD, et al. Impaired Chronotropic and Vasodilator Reserves Limit Exercise Capacity in Patients With Heart Failure and a Preserved Ejection Fraction. Circulation. 2006 Nov 14; 114(20): 2138-47.

[3] Tan YT, Wenzelburger F, Lee E, et al. The pathophysiology of heart

failure with normal ejection fraction: exercise echocardiography reveals complex abnormalities of both systolic and diastolic ventricular function involving torsion, untwist, and longitudinal motion. J Am Coll Cardiol. 2009 Jun 30; 54(1): 36-46.

[4] Knegt MC de, Biering-Sorensen T, Sogaard P, et al. Concordance and reproducibility between M-mode, tissue Doppler imaging, and two-dimensional strain imaging in the assessment of mitral annular displacement and velocity in patients with various heart conditions. Eur Heart J - Cardiovasc Imaging. 2013 Jun 28; jet119.

[5] Willenheimer R, Israelsson B, Cline C, et al. Left atrioventricular plane displacement is related to both systolic and diastolic left ventricular performance in patients with chronic heart failure. Eur Heart J. 1999 Apr 1; 20(8): 612-8. PMid:10337546. https://doi.org/10.1053/euhj.1998.1399

[6] Hu K, Liu D, Herrmann S, et al. Clinical implication of mitral annular plane systolic excursion for patients with cardiovascular disease. Eur Heart J Cardiovasc Imaging. 2013 Mar 1; 14(3): 205-12.

[7] Biering-Sørensen T, Solomon SD. Assessing Contractile Function When Ejection Fraction Is Normal. Circ Cardiovasc Imaging. 2015 Nov 1; 8(11): e004181. PMid:26546484. https://doi.org/10.1161/CIRCIMAGING.115.004181

[8] Wang J, Khoury DS, Yue Y, et al. Preserved left ventricular twist and circumferential deformation, but depressed longitudinal and radial deformation in patients with diastolic heart failure. Eur Heart J. 2008 May 1; 29(10): 1283-9. PMid:18385117.

[9] Ersbøll M, Andersen MJ, Valeur N, et al. Early diastolic strain rate in relation to systolic and diastolic function and prognosis in acute myocardial infarction: a two-dimensional speckle-tracking study. Eur Heart J. 2014 Mar 7; 35(10): 648-56.

[10] Hung CL, Verma A, Uno H, et al. Longitudinal and circumferential strain rate, left ventricular remodeling, and prognosis after myocardial infarction. J Am Coll Cardiol. 2010 Nov 23; 56(22): 1812-22.

[11] Eto Y, Yamada H, Shin JH, et al. Automated mitral annular tracking: A novel method for evaluating mitral annular motion using two-dimensional echocardiography. J Am Soc Echocardiogr. 2005 Apr 1; 18(4): 306-12.

[12] Nevo ST, Stralen M van, Vossepoel AM, et al. Automated Tracking of the Mitral Valve Annulus Motion in Apical Echocardiographic Images Using Multidimensional Dynamic Programming. Ultrasound Med Biol. 2007 Sep 1; 33(9): 1389-99.

[13] Voigt JU, Pedrizzetti G, Lysyansky P, et al. Definitions for a common standard for 2D speckle tracking echocardiography: consensus document of the EACVI/ASE/Industry Task Force to standardize deformation imaging. Eur Heart J Cardiovasc Imaging. 2014 Dec 18; jeu184.

[14] Lang RM, Badano LP, Mor-Avi V, et al. Recommendations for Cardiac Chamber Quantification by Echocardiography in Adults: An Update from the American Society of Echocardiography and the European Association of Cardiovascular Imaging. J Am Soc Echocardiogr. 2015 Jan 1; 28(1): 1-39.e14.

[15] Loizou CP, Theofanous C, Pantziaris M, et al. Despeckle filtering software toolbox for ultrasound imaging of the common carotid artery. Comput Methods Programs Biomed. 2014 Apr 1; 114(1): 109-24. PMid:24560276. https://doi.org/10.1016/j.cmpb.2014.01.018

[16] Coupe P, Yger P, Prima S, et al. An optimized blockwise nonlocal means denoising filter for 3-D magnetic resonance images. IEEE Trans Med Imaging. 2008 Apr; 27(4): 425-41. PMid:18390341. https://doi.org/10.1109/TMI.2007.906087

[17] Yeung F, Levinson SF, Fu D, et al. Feature-adaptive motion tracking of ultrasound image sequences using a deformable mesh. IEEE Trans Med Imaging. 1998 Dec; 17(6): 945-56. PMid:10048851. https://doi.org/10.1109/42.746627

[18] Kalal Z, Mikolajczyk K, Matas J. Forward-Backward Error: Automatic Detection of Tracking Failures. In: 2010 20th International Conference on Pattern Recognition. 2010. p. 2756-9.

[19] Chowdhury SM, Butts RJ, Taylor CL, et al. Abstract 10876: Speckle-tracking vs. Pressure-Volume Loop Measures of Left Ventricular Systolic Function in Children: An Inter-vendor Comparison. Circulation. 2015 Nov 10; 132(Suppl 3): A10876.

[20] Cameli M, Caputo M, Mondillo S, et al. Feasibility and reference values of left atrial longitudinal strain imaging by two-dimensional speckle tracking. Cardiovasc Ultrasound. 2009; 7: 6. PMid:19200402. https://doi.org/10.1186/1476-7120-7-6

[21] Suffoletto MS, Dohi K, Cannesson M, et al. Novel Speckle-Tracking Radial Strain From Routine Black-and-White Echocardiographic Images to Quantify Dyssynchrony and Predict Response to Cardiac Resynchronization Therapy. Circulation. 2006 Feb 21; 113(7): 960-8. PMid:16476850. https://doi.org/10.1161/CIRCULATIONAHA.105.571455

[22] Luszczak J, Olszowska M, Drapisz S, et al. Assessment of left ventricle function in aortic stenosis: mitral annular plane systolic excursion is not inferior to speckle tracking echocardiography derived global longitudinal peak strain. Cardiovasc Ultrasound. 2013; 11: 45. PMid:24373119. https://doi.org/10.1186/1476-7120-11-45

[23] Keramida K, Kouris N, Kostopoulos V, et al. Differences of left ventricular 2d strain curves in patients with dilated and ischemic cardiomyopathy. Eur J Heart Fail [Internet]. 2014 May 1 [cited 2017 Jan 21]; 16. Available from: http://insights.ovid.com/european-heart-failure/ejhf/2014/05/002/differences-left-ventricular-2d-strain-curves/232/00127070

[24] Kempny A, Diller GP, Kaleschke G, et al. Longitudinal left ventricular 2D strain is superior to ejection fraction in predicting myocardial recovery and symptomatic improvement after aortic valve implantation. Int J Cardiol. 2013 Sep 1; 167(5): 2239-43.

[25] Haruki N, Takeuchi M, Gerard O, et al. Accuracy of measuring mitral annular velocity by 2D speckle tracking imaging. J Cardiol. 2009 Apr; 53(2): 188-95.

[26] Bellman RE, Dreyfus SE. Applied Dynamic Programming. Princeton University Press; 2015. 389 p.

[27] Casazza F, Bongarzoni A, Capozi A, et al. Regional right ventricular dysfunction in acute pulmonary embolism and right ventricular infarction. Eur Heart J - Cardiovasc Imaging. 2005 Jan 1; 6(1): 11-4.